

# Half-metallic Antiferromagnet Sheets in $\text{Sr}_4\text{M}_2\text{O}_6\text{CrFeAs}_2$ ( $\text{M}=\text{Sc}, \text{Cr}$ ) and Their Bulk Form

Shu-Jun Hu and Xiao Hu

World Premier International Center for Materials Nanoarchitectonics (MANA)  
National Institute for Materials Science, Tsukuba 305-0044, Japan

(Dated: March 22, 2022)

We reveal by first-principles calculations that in iron pnictides  $\text{Sr}_4\text{M}_2\text{O}_6\text{CrFeAs}_2$  ( $\text{M}=\text{Sc}, \text{Cr}$ ) the two-dimensional  $\text{CrFeAs}_2$  layers exhibit a robust band structure of half-metallic antiferromagnet (HMAFM). Due to the thick blocking layer, the interlayer coupling is vanishingly small and thus the conductive channels in individual layers may take the alternative spin direction randomly. We show that, since the spin magnetizations of Fe and Cr are different in a ferromagnetic state, applying a strong magnetic field and ramping it down gradually can align the spin direction of conductive channel of all HMAFM layers, which restores the bulk HMAFM.

PACS numbers: 74.70.Xa, 85.75.-d, 31.15.A-

Spin is one of the fundamental properties of electron. Exploitation of the spin-dependent transportation, dubbed as spintronics, which emerged from the discovery of giant magnetoresistance effect [1, 2], has been a topic of particular interest in the last decades. Generation of the spin-polarized current is the primary requirement of spintronics devices. Half metals [3], a class of materials possess states in only one spin channel at the Fermi level ( $E_F$ ), have received considerable attention since they yield fully spin-polarized currents.

Owing to the asymmetric electron populations in the two spin channels, half metals are often ferromagnetic (FM) or ferrimagnetic. Half-metallic antiferromagnet (HMAFM) materials proposed first by van Leuken and de Groot[4] should be superior in many applications, where stray fields are harmful, since they achieve fully spin-polarized currents without showing net magnetization. To date, many HMAFM candidates have been engineered by the first-principles calculations based on the double perovskite compounds [5–7] and Heusler alloys [8]. Besides, HMAFM have been predicted by doping in oxide semiconductor [9], transition-metal (TM) oxides [10] and cuprate[11].

In a previous study[12], the present authors proposed to achieve HMAFM based on the recently renaissance iron pnictides [13]. We substituted half of the Fe atoms by Cr in  $\text{BaFe}_2\text{As}_2$ . The ground state was characterized by the following properties: the Fe and Cr atoms form intervening three-dimensional (3D) lattice, the spin magnetizations of Fe, Cr and As compensate completely, and close to  $E_F$  the states are contributed exclusively from the spin channel of Cr:3d majority electrons. The material  $\text{BaFe}_2\text{As}_2$  is therefore predicted as a HMAFM.

In the present work, we focus on the recently discovered iron pnictides  $\text{Sr}_4\text{M}_2\text{O}_6\text{Fe}_2\text{As}_2$  ( $\text{M}=\text{Sc}, \text{Cr}$ ) [14]. These new iron pnictides (see also [15, 16]) are unique in the structure where the FeAs layers are separated by layers of perovskite structure as thick as  $9.8 \text{ \AA}$ , and thus is much more two-dimensional (2D) than other iron pnictides. We substitute half of the Fe atoms by the conjugate element Cr as revealed in Ref.[12]. From

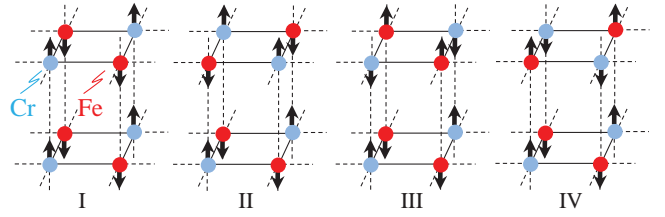


FIG. 1. (Color online) Lattice and spin orders of four degenerated configurations of TM layers in the ground state of  $\text{Sr}_4\text{Sc}_2\text{O}_6\text{CrFeAs}_2$ . The As ions and blocking layers in the unit cell are omitted for a clear view. Configuration I and II, in which all Cr (and Fe) ions take the same spin direction, are predicted to be HMAFM, while III and IV are not.

first-principles calculations it becomes clear that in the ground state the individual TM pnictide ( $\text{CrFeAs}_2$ ) layers take the checkerboard order of Cr and Fe ions associated with the antiferromagnetic (AFM) spin order, and exhibit HMAFM electronic structure. Due to the vanishing interlayer coupling, both lattice and spin disorders easily appear in the  $c$  direction, which suppresses the bulk HMAFM property. Interestingly, it is found that the spin magnetizations of Cr ions are much larger than Fe ions in the FM state. Therefore, a post-process of applying a strong magnetic field and ramping down gradually can restore the spin order along the  $c$  direction and thus achieve the 3D HMAFM. The present approach to achieve the bulk property based on the robust 2D one prepared in advance may shed light for future exploration of HMAFM.

The calculations are performed using the projector augmented-wave (PAW) method [17] as implemented in the VASP simulation package [18, 19], with the generalized gradient approximation in PBE type [20] for the exchange-correlation functionals. The crystal structures of the parent materials revealed experimentally [14] are implemented in the present calculations for the doped system. Structure optimization is then performed using  $8 \times 8 \times 2$  Monkhorst-Pack [21] k-point mesh until the

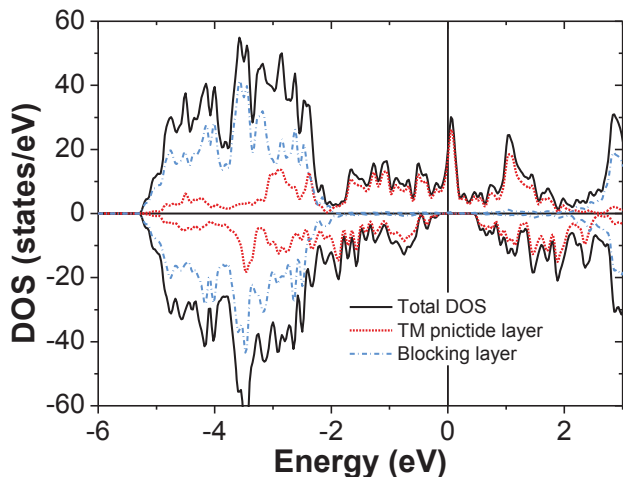


FIG. 2. (Color online) Total density of states (DOS) and those projected on the TM pnictide layer and blocking layer of  $\text{Sr}_4\text{Sc}_2\text{O}_6\text{CrFeAs}_2$ , respectively, for the atomic and spin orders I and II in Fig. 1.

TABLE I. Spin magnetizations of Cr, Fe and As ions and total spin magnetization (a) in states I and II shown in Fig. 1 and (b) in the FM state (units:  $\mu_B$ ). The total spin magnetization is obtained by integrating charge densities of both spin channels.

| Conf. | Cr   | Fe    | As    | $M_{tot}$ |
|-------|------|-------|-------|-----------|
| (a)   | 2.83 | -2.68 | -0.08 | 0.00      |
| (b)   | 2.45 | 0.56  | -0.08 | 11.33     |

stress of the supercell and the force of the ions are less than 1 kbar and  $10^{-3}$  eV/Å.

We begin with the identification of ground state of  $\text{Sr}_4\text{Sc}_2\text{O}_6\text{CrFeAs}_2$  by calculating the total energies of possible configurations within the  $\sqrt{2} \times \sqrt{2} \times 2$  supercell. The checkerboard configuration of Cr and Fe ions associated with AFM spin magnetizations is of energy lower than other 2D configurations at least by 0.23 eV. The robust in-plane checkerboard order is consistent with the case of  $\text{BaCrFeAs}_2$  [12], but in sharp contrast with the study for the '1111' system [22].

On the other hand, due to the diminished coupling across the thick blocking layer, the four configurations shown in Fig. 1 with different orders along the  $c$  axis possess almost the same energy ( $\Delta E \leq 3$  meV).

Figure 2 shows the total density of states (DOS) and those projected to the block layer and  $\text{CrFeAs}_2$  layer, for the configurations I and II in Fig. 1, where the Cr (Fe) 3d majority electrons are spin-up (spin-down). The band near  $E_F$  (from -2 to 1 eV) is dominated by states from  $\text{CrFeAs}_2$  layers, and all the occupied states from the blocking layer are deep in the valence band. This result reveals the role of blocking layer as the charge reservoir. At  $E_F$  the DOS is exclusively contributed by the spin-up states, which consist of the Cr:3d majority and Fe:3d

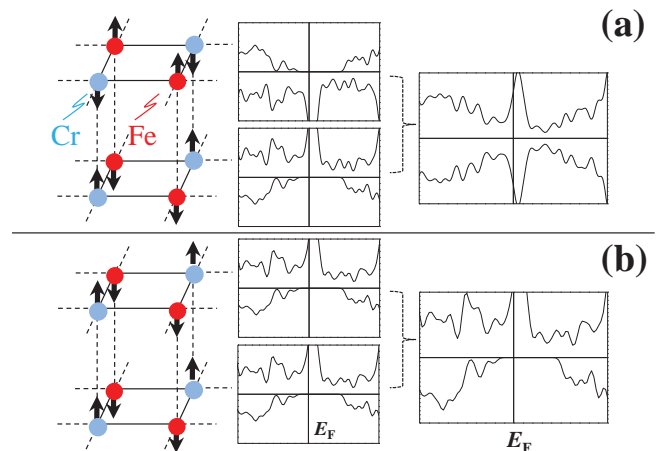


FIG. 3. (Color online) From (a) the state III in Fig. 1 (2D HMAFM) to (b) a bulk HMAFM. Left column: lattice and spin orders; center column: DOSs of individual TM layers; right column: total DOS. DOSs are shown in energy range from -1 to 1 eV relative to  $E_F$ .

minority electrons, and a part of As:4p states. As illustrated in Table I, the total magnetization is zero due to the complete compensation of the spin magnetizations of Cr, Fe and As ions. Therefore, the material is a HMAFM in the states I and II shown in Fig. 1.

In  $\text{BaCrFeAs}_2$  [12], the strong interlayer coupling via the direct As bonding delocalizes the As:4p states, resulting a narrow band gap of 0.3 eV. In  $\text{Sr}_4\text{Sc}_2\text{O}_6\text{CrFeAs}_2$ , the coupling is diminished due to the thick blocking layer. Therefore, the As:4p states are well confined in the  $\text{CrFeAs}_2$  layer. The energy gap of  $\text{Sr}_4\text{Sc}_2\text{O}_6\text{CrFeAs}_2$  is calculated to be 0.7 eV, which is much larger than that of  $\text{BaCrFeAs}_2$ .

For the configuration III in Fig. 1, the total DOS is symmetric in the two spin channels, as shown in the right column of Fig. 3(a). However, projecting the total DOS on the blocking layers and the two individual TM pnictide layers, we find that, first, the blocking layers still do not contribute to states close to  $E_F$ , and secondly, the two TM pnictide layers are HMAFM with the metallic channels in opposite spin directions, as shown in the center column of Fig. 3(a). The same results are obtained for configuration IV in Fig. 1. Therefore,  $\text{Sr}_4\text{Sc}_2\text{O}_6\text{CrFeAs}_2$  shows a robust 2D HMAFM, while the bulk HMAFM may be suppressed due to the degenerated states of different spin orders along the  $c$  axis.

Since the spin order can be tuned by external magnetic field, we investigate the property of FM spin configuration, which is achieved when the external magnetic field is strong enough. It is revealed by first-principles calculations that in the FM state the spin magnetization of Cr is much larger than that of Fe as displayed in Table I, in a sharp contrast to the AFM state where they are almost the same. The difference in the spin magnetizations, and thus in the Zeeman energies, can be used to tune the spin orders. In a strong magnetic field overcoming the

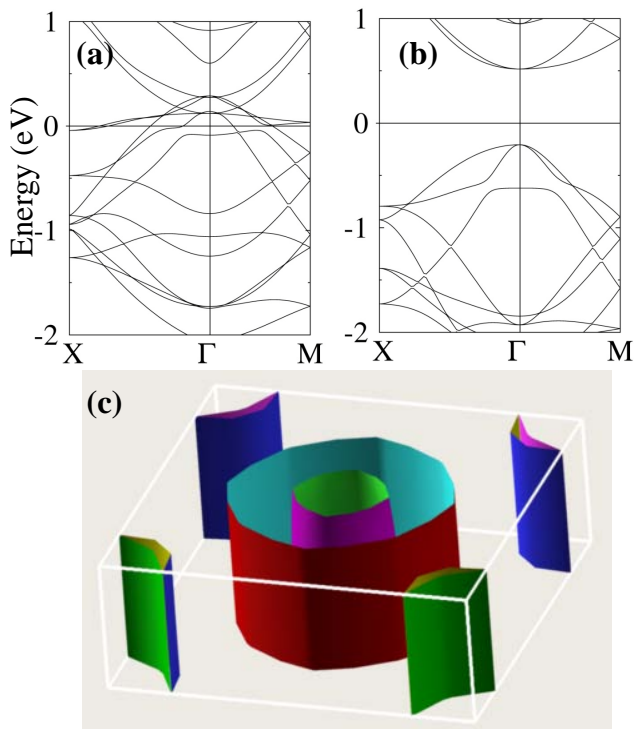


FIG. 4. (Color online) Band structure of  $\text{Sr}_4\text{Sc}_2\text{O}_6\text{CrFeAs}_2$ . (a) spin-up band; (b) spin-down band. (c) Fermi surfaces of the spin-up band.

energy difference between the FM and AFM states, the spin magnetizations of both Cr and Fe are simply aligned along the external field. During the process of ramping the external field down to zero, the spin magnetization of Fe flips to the direction opposite to the external field, since the spin magnetization of Fe presumes smaller Zeeman energy and the AFM state is much more stable than the FM state. Thus, no matter what the initial c-axis spin order is, the AFM order between Cr and Fe can be restored over the bulk material as shown in Fig. 3(b). The 3D HMAFM property is eventually achieved.

We then look at the band structure of 3D HMAFM  $\text{Sr}_4\text{Sc}_2\text{O}_6\text{CrFeAs}_2$ . For the configuration I in Fig. 1, we use a  $\sqrt{2} \times \sqrt{2} \times 1$  supercell to perform the calculation. As displayed in Fig. 4(a), the partially occupied bands in the spin-up channel include two hole bands contributed by the TM: $t_{2g}$  electrons and two almost degenerated Fe: $d_{3z^2-r^2}$  bands corresponding to the peak in DOS near  $E_F$  in Fig. 2. The Fermi surfaces of the spin-up channel are shown in Fig. 4(c). The hole pockets near the  $\Gamma$  point are induced by the TM: $t_{2g}$  states and two Fermi surfaces near the X points of the Brillouin zone are contributed by the Fe: $d_{3z^2-r^2}$  states. All the Fermi surfaces show a more significant 2D character as compared with the iron-pnictides with thinner blocking layers [23]. There is no Fermi surface in the spin down channel since a gap is opened.

First-principles calculations reveal that the band structure of configuration II is almost the same as that of

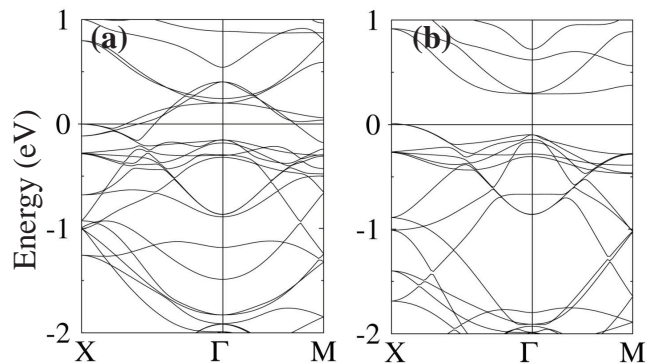


FIG. 5. Band structure of  $\text{Sr}_4\text{Cr}_2\text{O}_6\text{CrFeAs}_2$ . (a) spin-up band; (b) spin-down band.

configuration I, both characterized by the same Cr (Fe) spin direction over the bulk. Therefore, we predict that, as an aggregate of configurations I and II, the bulk  $\text{Sr}_4\text{Sc}_2\text{O}_6\text{CrFeAs}_2$  subjected to the processing of an external field is of the same band structure as shown in Fig. 4.

Next let us address whether Cr atoms in  $\text{Sr}_4\text{Sc}_2\text{O}_6\text{CrFeAs}_2$  would go to the blocking layers. In the blocking layer, only Sc atoms might be substituted by Cr, which forms the  $\text{Cr}_{\text{Sc}}\text{-Sc}_{\text{Cr}}$  anti-site defects. Using a  $2\sqrt{2} \times 2\sqrt{2} \times 1$  supercell we calculate the formation energy of anti-site defect, which is estimated to be as large as 2.41 eV. The  $\text{Cr}_{\text{Sc}}\text{-Sc}_{\text{Cr}}$  anti-site defect is thus effectively prohibited even the synthesizing temperature reaches 1500 K [14]. Therefore, the doped Cr ions prefer exclusively the Fe sites.

Finally we turn to the twin parent material  $\text{Sr}_4\text{Cr}_2\text{O}_6\text{Fe}_2\text{As}_2$ , where the Cr atoms exclusively occupy the B-sites of perovskite structure in the blocking layer [14]. In order to manipulate the band structures, we try the same approach, namely replacing half of the Fe atoms with Cr atoms in the FeAs layers. We find that in  $\text{CrFeAs}_2$  sheets the Fe and Cr atoms prefer the checkerboard distribution associated with an AFM order among Fe and Cr ions same as the case of  $\text{Sr}_4\text{Cr}_2\text{O}_6\text{CrFeAs}_2$ , and that Cr ions in the blocking layers form AFM order themselves consistently with the experimental observation [24]. As shown in Fig. 5, the material  $\text{Sr}_4\text{Cr}_2\text{O}_6\text{CrFeAs}_2$  has a gap in the spin-down channel and is metallic in the spin-up channel, and thus is predicted to be another HMAFM. The gap is 0.2 eV, smaller than the previous case since Cr atoms in the blocking layers yield additional bands around  $E_F$ . In the majority band, the orbitals  $d_{yz}$ ,  $d_{xz}$  and  $d_{x^2-y^2}$  of Cr atoms are fully occupied, while the other two orbitals are well above  $E_F$  due to the Coulomb repulsion between them and p electrons of oxygen; all 3d orbitals in the minority band are empty.

To summarize, we reveal by first-principles calculations that in iron pnictides  $\text{Sr}_4\text{Sc}_2\text{O}_6\text{CrFeAs}_2$  and  $\text{Sr}_4\text{Cr}_2\text{O}_6\text{CrFeAs}_2$  the  $\text{CrFeAs}_2$  layers exhibit a robust, two-dimensional property of half-metallic antiferromag-

net. Although the weak interlayer coupling may allow spin disorders along the  $c$  axis, the antiferromagnetic spin order between Cr and Fe can be restored over the bulk material by applying a pulse of external magnetic field, which gives rise to three-dimensional half-metallic anti-

ferromagnet.

*Acknowledgements* – The calculations were performed on Numerical Materials Simulator (SGI Altix) of NIMS. This work was supported by WPI Initiative on Materials Nanoarchitectonics, MEXT, and partially by Grants-in-Aid for Scientific Research (No.22540377), Japan.

- 
- [1] G. Binasch, P. Grünberg, F. Saurenbach, and W. Zinn, *Phys. Rev. B* **39**, 4828 (1989).
  - [2] M. N. Baibich, J. M. Broto, A. Fert, F. N. Van Dau, F. Petroff, P. Eitenne, G. Creuzet, A. Friederich, and J. Chazelas, *Phys. Rev. Lett.* **61**, 2472 (1988).
  - [3] I. Galanakis and P. Dederichs, *Half-metallic alloys: fundamentals and applications* (Springer, Berlin, 2005).
  - [4] H. van Leuken and R. A. de Groot, *Phys. Rev. Lett.* **74**, 1171 (1995).
  - [5] W. E. Pickett, *Phys. Rev. B* **57**, 10613 (1998).
  - [6] J. H. Park, S. K. Kwon, and B. I. Min, *Phys. Rev. B* **65**, 174401 (2002).
  - [7] Y. K. Wang and G. Y. Guo, *Phys. Rev. B* **73**, 064424 (2006).
  - [8] K. Özdoğan, I. Galanakis, E. Şaşıoğlu, and B. Aktas, *J. Phys.: Condens. Matter* **18**, 2905 (2006).
  - [9] H. Akai and M. Ogura, *Phys. Rev. Lett.* **97**, 026401 (2006).
  - [10] D. Ködderitzsch, W. Hergert, Z. Szotek, and W. M. Temmerman, *Phys. Rev. B* **68**, 125114 (2003).
  - [11] Y.-M. Nie and X. Hu, *Phys. Rev. Lett.* **100**, 117203 (2008).
  - [12] S. Hu and X. Hu, *J. Phys. Chem. C* **114**, 11614 (2010).
  - [13] Y. Kamihara, T. Watanabe, M. Hirano, and H. Hosono, *J. Am. Chem. Soc.* **130**, 3296 (2008).
  - [14] H. Ogino, Y. Katsura, S. Horii, K. Kishio, and J. Shimoyama, *Supercond. Sci. Technol.* **22**, 085001 (2009).
  - [15] X. Zhu, F. Han, G. Mu, B. Zeng, P. Cheng, B. Shen, and H.-H. Wen, *Phys. Rev. B* **79**, 024516 (2009).
  - [16] X. Zhu, F. Han, G. Mu, P. Cheng, B. Shen, B. Zeng, and H.-H. Wen, *Phys. Rev. B* **79**, 220512 (2009).
  - [17] P. E. Blöchl, *Phys. Rev. B* **50**, 17953 (1994).
  - [18] G. Kresse and J. Hafner, *Phys. Rev. B* **47**, 558 (1993).
  - [19] G. Kresse and J. Furthmüller, *Phys. Rev. B* **54**, 11169 (1996).
  - [20] J. P. Perdew, K. Burke, and M. Ernzerhof, *Phys. Rev. Lett.* **77**, 3865 (1996).
  - [21] H. J. Monkhorst and J. D. Pack, *Phys. Rev. B* **13**, 5188 (1976).
  - [22] M. Nakao, *J. Phys.: Conf. Ser.* **150**, 052182 (2009).
  - [23] H. Nakamura, M. Machida, T. Koyama, and N. Hamada, *J. Phys. Soc. Jpn.* **78**, 123712 (2009).
  - [24] M. Tegel, F. Hummel, Y. Su, T. Chatterji, M. Brunelli, and D. Johrendt, *Europhys. Lett.* **89**, 37006 (2010).